crystals

MDPI

Article

A New Charge-Ordered Molecular Conductor: κ-(BEDT-TTF)$_2$K$^+$(18-crown-6)[Co^{II}(NCS)$_4$]·(H$_2$O)

Andrei A. Bardin [1,2,*], Tatiana G. Prokhorova [3] and Lev I. Buravov [3]

[1] Center for Applied Structural Discovery, Biodesign Institute, Arizona State University, 727 East Tyler Street, Tempe, AZ 85287, USA
[2] School for Engineering of Matter, Transport and Energy, Arizona State University, Tempe, AZ 85287, USA
[3] Federal Research Center of Problems of Chemical Physics and Medicinal Chemistry, Russian Academy of Sciences, 142432 Chernogolovka, Russia; prokh@icp.ac.ru (T.G.P.); buravov@icp.ac.ru (L.I.B.)
* Correspondence: dr.abardin@gmail.com or andrei.bardin@asu.edu

Abstract: A new molecular conductor, i.e., κ-(BEDT-TTF)$_2$K$^+$(18-crown-6)[Co^{II}(NCS)$_4$]·(H$_2$O), is semiconductive with substantial charge gap values (ΔE) of 0.57 eV (measured) and 0.37 eV (calculated). There is a full band separation despite formal average charge on BEDT-TTF of +0.5 and κ(kappa)-type packing of BEDT-TTF dimers that favors high conductivity. X-ray crystal structure analysis reveals complete charge ordering with full Coulomb charge on unique BEDT-TTF radical cations ***A*** (Q_A = +1), while unique molecules ***B*** are uncharged (Q_B = 0). Geometries of ***A*** (flat) and ***B*** (bent) differ considerably and are in accordance with the ascribing charges. Charge segregation is enhanced by forming tight face-to-face BEDT-TTF dimers ***AA*** (Q_{AA} = +2) and ***BB*** (Q_{BB} = 0). Strongly interacting double-charged dimers ***AA*** form "superstripes" running along ***a*** that are interleaved along ***b*** with chains of neutral dimers ***BB***. Peculiar extremely thick (13.7 Å) four-decker insulating anion layers cast strong Coulomb potential onto the conductive layers predetermining charge localization in the latter.

Keywords: single-molecule magnet (SMM); charge ordering (CO); stripe order; metal-insulator (MI) transition; molecular conductors; electrocrystallization; single-crystal X-ray diffraction (SXRD); extended Hückel tight-binding (EHTB) calculations; four-probe conductivity measurement

Citation: Bardin, A.A.; Prokhorova, T.G.; Buravov, L.I. A New Charge-Ordered Molecular Conductor: κ-(BEDT-TTF)$_2$K$^+$(18-crown-6)[Co^{II}(NCS)$_4$]·(H$_2$O). *Crystals* **2023**, *13*, 1504. https://doi.org/10.3390/cryst13101504

Academic Editor: Andrej Pustogow

Received: 31 August 2023
Revised: 6 October 2023
Accepted: 11 October 2023
Published: 16 October 2023

1. Introduction

The investigation of single-molecule magnets (SMMs) is a very hot topic in contemporary science. This is explained by an extreme density of data potentially attained in electromechanical data storage devices, where SMMs are employed for the construction of magnetic carrier layers. Moreover, combining advances of SMMs with electrical conductivity provides a roadmap for future devices, where spins are controlled by electric current or where the current is measured to detect of spin state change. Recently, simple compounds of composition [K$^+$(18-crown-6)]$_2$Co^{II}(NCS)$_4$ and [Ba^{2+}(18-crown-6)(H$_2$O)$_3$]Co^{II}(NCS)$_4$ were proven to demonstrate slow relaxation of magnetic moment, which is a key property for the realization of an SMM state [1]. SMM properties in these materials are introduced by tetrahedral cobalt dianion Co^{II}(NCS)$_4^{2-}$ and the cation part serves only charge balancing purposes.

It was of extreme interest to replace cationic sublattice by another that benefits entire lattice by extra advantageous physical properties, such as electrical conductivity.

We used an organic single-electron donor BEDT-TTF (Bis(ethylenedithio)tetrathiafulvalene, or, for extra brevity, ET), which is known to give conductive crystals with various anions, where BEDT-TTF (ET) acts as a radical cation with formally fractional charge (most frequently +0.5) (Scheme 1).

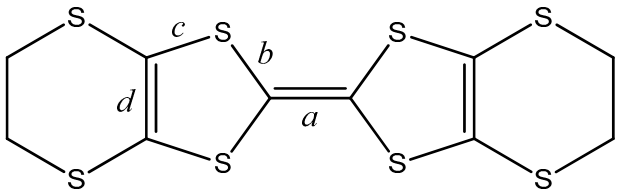

Scheme 1. Structural formula of BEDT-TTF (ET).

The crystal structure of ET salts is layered, where ET radical cation layers, responsible for electrical conductivity, are alternated with anionic layers, usually insulating. This spatial segregation of anionic and cationic counterparts is a handy tool that allows performing contemporary crystal engineering approaches to introduce a variety of desired physical properties manipulating independently with anionic and cationic sublattices. There is a certain advantage of BEDT-TTF over other known organic electron donors consisting of a great variety of possible ET layer patterns in produced conductive salts.

There is a well-developed rational nomenclature of known packing types for existing ET salts, traditionally labeled by Greek letters preceding the formula (α-, β-, δ-, θ-, κ-, etc. [2–4]), concerning mainly a mutual ET arrangement within the layer, which, however, lacks the rationales concerning structural features that are perpendicular to ET conductive layers. It is known that packing type of ET layers has a strong influence on the physical properties, such as conductivity [5]. Differently packed salts demonstrate various conductive properties, ranging from insulating up to superconductivity.

One of the ET layer packing types attracting particular interest is a so-called κ (kappa) type, where neighboring ET face-to-face dimers are situated in a checkerboard order tilting by an angle that is close to 90° (Figure 1) [3]. In the current report, we update the rational nomenclature for ET κ-salts by thorough analysis of mutual arrangements and repeating motifs of ET radical cations in the dimension that is perpendicular to the layer expansion one. Previously, we performed a similar update for the conductive κ salts of another organic single electron donor—BDH (vide infra) [6].

It was a κ-type compound κ-$ET_2Cu(NCS)_2$ that opened an era of "high temperature" (T_c > 10 K) ambient pressure organic superconductivity (T_c = 10.9 K) [7]. Thanks to the crystal lattice softness of organic compounds, their electronic state is able to be adjusted by mechanical strain [8]. κ-$ET_2Cu_2(CN)_3$ single crystals strained on SiO_2 substrate made it possible to obtain an ambipolar superconducting field-effect transistor operating above liquid helium temperature [9]. Moreover, another ET κ-salt, namely, κ-$ET_2Cu[N(CN)_2]Br$, still keeps a temperature record for ambient pressure superconductivity in radical cation salts with the T_c onset value of 12 K [10]. Besides its robust superconductive state, a thorough survey of in-plane superfluid density and microwave conductivity revealed evidence for *d*-wave pairing and resilient quasiparticles [11]. This confirmed the non-BCS (Bardeen-Cooper-Schrieffer) unconventional *d*-wave character of the superconductivity state in organic charge transfer salts, which had been questioned for a long time [12–14]. The elusive quantum spin liquid state in organic charge transfer salts was also initially discovered in κ-$ET_2Cu_2(CN)_3$ [15–18]. Further investigations revealed a gapped magnetic ground state in this quantum spin liquid candidate [19]. The latter has also finely tuned the superconductive dome adjustable by donor layer alloying [20]. κ-Type packing is typical not only for ET salts, but also for the structural isomer of ET—BDH (2,5-bis(1,3-dithiolan-2-ylidene)-1,3,4,6-tetrathiapentalene). The molecular structure of BDH is related to ET by a 90° rotation of all three C=C bonds [21].

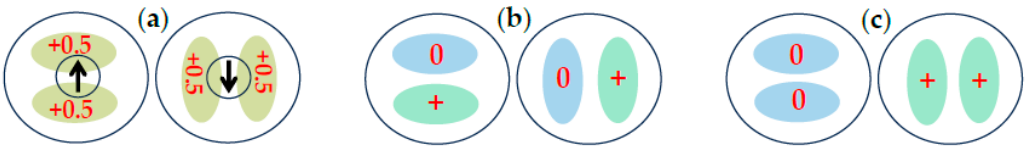

Figure 1. Various patterns of charge distribution over BEDT-TTF molecules packed into orthogonal ET dimers (denoted by large circles) within conductive layers. Simplified projection along long molecular axis of BEDT-TTF. (**a**) Mott antiferromagnetic insulator state (distinct spins exemplified by upright and upside-down arrows in small circles) [22]. (**b**) Intradimer charge-ordered (CO) state. (**c**) Interdimer CO state.

Moreover, the κ-arrangement is dominant in conductive BDH salts. Unlike ET salts, the electronic state of κ-BDH salts is less dependent from the employed anions and the great majority of κ-BDH salts are stable metals [6]. This less correlative behavior of κ-BDH salts, on the one hand, benefits the family by an abundance of highly conductive compounds with various paramagnetic anions, leading to the lack of superconductivity and other peculiar electronic states on the other.

Strong electronic correlations hosting in ET-salts give rise to various types of electronic instabilities [23], in turn providing a plethora of various physical phenomena besides unconventional superconductivity and quantum spin liquid [24–26]. Among them are colossal magnetoresistance, Mott criticality [27–30], Mott metal-insulator (MI) transition [31–33], ferroelectricity, multiferroicity [34], and charge ordering (CO) [35]. The latter has attracted much attention recently, both from the fundamental point of view and possible further applications. As an example, CO-driven ferroelectricity was proposed in ET charge transfer salts of various packing types [36], such as κ-$ET_2Cu[N(CN)_2]Cl$ [34] and α-ET_2I_3 [37–40]. Recently, it was found that CO phenomena play important role in the complex conductivity behavior of chiral molecular conductor based on the methylated ET (BEDT-TTF) donor analogue—κ-$[(S,S)\text{-DM-BEDT-TTF}]_2ClO_4$ [41].

However, CO phenomena were mainly observed and deeply investigated in ET θ-phase [42]. These instances are most notably exemplified by the family members of θ-$ET_2MM'(SCN)_4$ ($M = Rb^+$, Tl^+, Cs^+; $M' = Zn^{2+}$ or Co^{2+}) [43,44], where electronic properties are mainly governed by monoanions M. Remarkable examples of CO due to intermolecular interactions leading by Coulomb forces are θ-$ET_2RbZn(SCN)_4$ [45] and θ-$ET_2RbCo(SCN)_4$ [46]. These isostructural salts are characterized by the spatial pattern called "stripe order", where ET radical cations of different ionicity form parallel chains [47]. In this particular case, horizontal stripes alternating along axis **c** are realized. These salts exhibit a first-ordered MI structural phase transition below T_{MI} = 200 K from ***I*222** to $\boldsymbol{P2_12_12_1}$ space group accompanied with 2***c*** superlattice formation. Above the phase transition point, there is only one independent ET radical cation with the charge Q = +0.5; however, below T_{MI}, two crystallographically unique ET molecules, ***A*** and ***B***, with the ionicity estimated from the molecular shapes as Q = +0.8 to +1.0 (***A***) and Q = 0 to +0.2 (***B***) were sensed along with the sudden drop of conductivity.

While widely presented in 3/4-filled θ-salts, in the κ-family, where the upper band is usually half-filled, the CO phenomena are very rare, and only a few compounds have been reported. Until recently, only two structures of this type were known—κ-$ET_4PtCl_6{\cdot}PhCN$ [48,49] and κ-$(ET)_4[M(CN)_6][Et_4N]{\cdot}2H_2O$ ($M = Co^{III}$, Fe^{III}) [50–52]. Their structure is rather complex: the phase transition includes the deformation of the molecule and the coupling to the anions; accordingly, details of their physical properties and their electronic states are not well known. Electronic correlations and coupling to the lattice vibrations undoubtedly play a major role in CO behavior. Thus, attempts of synthesizing of new κ-compounds with various types of CO states deserve additional efforts.

For insulating κ-phase, there are three possible ways to distribute positive charges over ET dimers and the resulting electronic states (Figure 1):

1. Mott state; ET radical cations are equally charged.

2. Intradimer CO; the charge is localized on one ET per dimer. This charge can be fixed or fluctuating.
3. Interdimer CO; two charges are located on one dimer (one charge per one ET), while another dimer is left uncharged.

Due to the lack of appreciable charge disproportionation in most of the commonly studied Mott insulators and quantum spin liquid compounds, a family of dimerized ET compounds has drawn particular attention, the κ-$ET_2Hg(SCN)_2X$ series, where X = Cl^-, Br^-, I^-, which was introduced 30 years ago by Lyubovskaya et al. [53–55]. Revisited quite recently, κ-$ET_2Hg(SCN)_2Cl$ demonstrated CO transition at 30 K, where the metal–insulator transition is linked to the magnetic order [56,57]. Afterward, MI transition at 80 K due to CO was shown for the isostructural salt κ-$ET_2Hg(SCN)_2Br$ [58,59]. Resilient quantum fluctuations of spin and electric dipole degrees of freedom were found in κ-$(BEDT\text{-}TTF)_2Hg(SCN)_2Br$ down to the lowest measured temperatures [60]. The electric dipoles presumably created by intradimer charge imbalance forming fluctuating intradimer CO state that is not detectable by crystallographic means [61]. No pronounced structural changes concomitant to the electronic phenomena were discovered for these cases.

In contrast, κ-$(ET)_4[M(CN)_6][Et_4N]\cdot 2H_2O$ salts demonstrated a transition at around 150 K from a Mott insulating phase with the fluctuation of charge order to a interdimer CO phase associated with drastic conformational deformations of two crystallographically independent ET molecules with an evenly distributed charge of +0.5 to the charge-ordered ground state containing a $(ET^0)_2$ bent and a $(ET^+)_2$ flat face-to-face dimers built solely from independent ET-s [50].

In the current report, we present conductive radical cation salt κ-$(BEDT\text{-}TTF)_2Co^{II}(NCS)_4[K^+(18\text{-crown-}6)]\cdot(H_2O)$ (**1**), possessing magnetic Co^{II} centers and demonstrating robust interdimer CO state. Preliminary magnetic measurements revealed some signs of an SMM state. Additional experiments are underway.

2. Materials and Methods

2.1. Electrocrystallization

Electrocrystallization of the charge transfer salt (**1**) was performed in conventional two-compartment H-shaped cells with Pt wire electrodes at constant current and temperature (25 °C). In total, 100 mg of preformed electrolyte $[K^+(18\text{-crown-}6)]_2Co^{II}(NCS)_4$ obtained by the published procedure of [1] and 20 mg of BEDT-TTF were dissolved in 30 mL of 1,2-dichloroethane containing 3 mL of 96% ethanol. The resulting solution was transferred to the cathode compartment of the cell under Ar conditions. The obtained solution was distributed between the two compartments of the cell. Constant current of 0.4 μA was used for three weeks to give well-shaped black single crystals in the form of elongated plates. Crystals were harvested from anode, rinsed by a mother solution and initial solvent mixture and used for conductivity and X-ray measurements.

2.2. X-ray Diffraction and Structural Analysis

X-ray diffraction analyses for a single crystal of salt **1** were carried out on a CCD Agilent Xcalibur diffractometer with an EOS detector (Agilent Technologies UK Ltd., Yarnton, Oxfordshire, UK). Data collection, determination, and refinement of unit cell parameters were carried out using the CrysAlis PRO program suite [62]. X-ray diffraction data at 100(1) K were collected using MoKα (λ = 0.71073 Å) radiation.

The structure was solved by the direct methods using SHELXT and refined against all F^2 data [63]. The positions and thermal parameters of non-hydrogen atoms were refined isotropically and then anisotropically by the full-matrix least-squares method. Positions of hydrogen atoms were obtained from difference Fourier syntheses and refined with riding model constraints using SHELXL [64]. All calculations were performed with the ShelXle program package [65]. Figures were prepared using programs SHELXLe and Mercury [66]. Searching in the CCDC database and retrieving structures were performed using ConQuest [67].

The X-ray crystal structure data have been deposited with the Cambridge Crystallographic Data Center, with reference code CCDC 2130914 (**1**).

2.3. Calculation of Transfer Integrals and Band Structure

The extended Hückel tight binding (EHTB) method with the effective one-electron potential was applied for band structure calculations using a freeware program package, CAESAR [68]. Computing the off-diagonal matrix elements, $\boldsymbol{H}_{ij} = \langle \chi_i | \boldsymbol{H}_{eff} | \chi_j \rangle$, was performed by the modified Wolfsberg–Helmholz weighted scheme [69]. Double-ζ Slater orbitals for C and S atoms, and single-ζ Slater orbitals for H atoms were employed to treat the valence electrons explicitly. The exponents (ζ_i and $\zeta_{i'}$), contraction coefficients (c_i and $c_{i'}$), and atomic ionization potentials $\boldsymbol{H}_{ii}$ were taken from previous work [70].

2.4. Resistivity Measurements

Four platinum wires were attached using carbon paint to the conductive surface of a single crystal. Constant current was applied to the outer wires and voltage drop was detected on the inner wires. Conductivity was measured from room down to liquid nitrogen temperature. Room temperature resistance and resistivity were 1.8 KΩ and 3 Ω·cm, respectively. Sample size was 1.4 × 1 × 0.03 mm.

3. Results and Discussion

3.1. Crystal Structure

Radical cation salt **1** has the stochiometric formula κ-(BEDT-TTF)$_2$K$^+$(18-crown-6)[Co^{II}(NCS)$_4$]·(H$_2$O) that crystallizes in the triclinic space group Pī, with two crystallographically independent BEDT-TTF (***A*** and ***B***) molecules, double-charged [Co^{II}(NCS)$_4$]$^{2-}$ anion, and potassium K$^+$ cation coordinated by a 18-crown-6 ether and a water molecule. The latter crystal lattice components form bulky single charged anion {K$^+$(18-crown-6)[Co^{II}(NCS)$_4$]·(H$_2$O)}$^-$ that counterbalances a single positive charge distributed over ***A*** and ***B*** radical cations. The structure of **1** is layered, where conducting radical cation layers are intervened between complex insulating anion layers (Figure 2a). Within the conductive layers, BEDT-TTF radical cations ***A*** and ***B*** are packed by the so-called κ (kappa) type, where centrosymmetrical face-to-face dimers ***AA*** and ***BB*** are situated in a checkerboard order (Figure 2b).

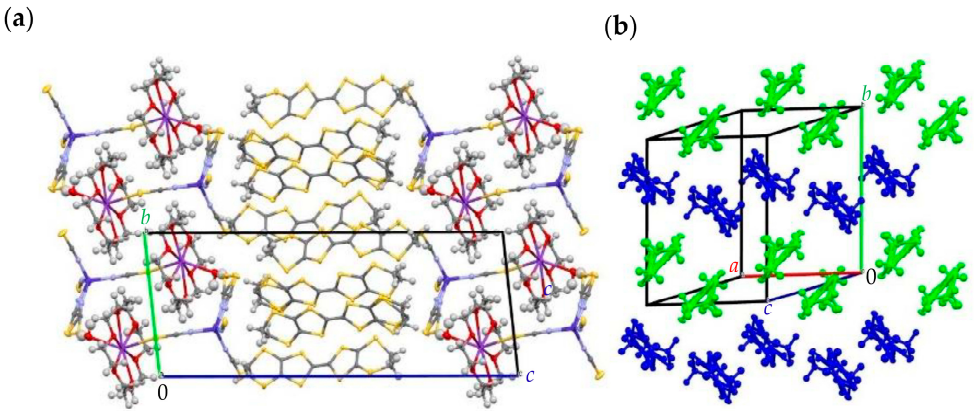

Figure 2. (**a**) Crystal structure of salt **1** κ-(BEDT-TTF)$_2$K$^+$(18-crown-6)[Co^{II}(NCS)$_4$] along the ***a*** axis. Carbon is dark gray, hydrogen is light gray, sulfur is yellow, oxygen is red, nitrogen is light blue, potassium is violet. (**b**) Conducting BEDT-TTF radical cation layers of salt **1** packed by κ-type. Crystallographically unique BEDT-TTF radical cations are denoted by color: ***A*** (green), ***B*** (blue).

Conductive organic and insulating inorganic layers alternate in the sequence [**I-II-III-III-II-I**-]$_\infty$ along axis ***c*** (Figure 2a), where **I** is a conducting radical cation BEDT-TTF organic layer, **II** is an anion layer, composed of double-charged anions Co(NCS)$_4^{2-}$, and **III** is a K$^+$(18-crown-6)·(H$_2$O) non-conductive cation layer that decreases the charge of

the former double-charged anion by one. Thus, the anion layer is organized similar to a pancake, where two positively charged K^+(18-crown-6)·(H_2O) layers **III** are situated inside this anionic [-**II**-**III**-**III**-**II**-] assembly. Anions $Co(NCS)_4^{2-}$, forming layers **II**, are rendered to its periphery, residing in a close proximity to the BEDT-TTF radical cations ***A***. That serves as an additional factor elevating the local Coulomb potential favoring charge localization in the conductive layers.

Such a complex organization of anion layers ends up with an anion layer thickness of 13.8 Å, which is the second highest value reported in the literature for layered BEDT-TTF salts (Table 1). It is worth mentioning that all compounds with record thicknesses of anion layers incorporate 18-crown-6 into the layer structure **1**–**3**, **5**. Interestingly, both top leaders demonstrate even more similarity containing potassium K^+ ion coordinated by crown ether and a water molecule. The anion layer thicknesses of circa 10 Å and above for crown-containing compounds, leaving behind values that are found in the compounds with huge chalcohalide rhenium clusters and Keggin polyoxoanions **6**, **7**. The only salt among compounds with the extreme anion thickness that does not contain 18-crown-6 (**4**), in fact, resembles crown-containing structures with a huge amount of included water molecules that replace crown ether for coordinating alkali sodium ions Na^+.

Table 1. Layer parameters for BEDT-TTF salts with the thickest anion layers (upper part) and κ-salts demonstrating charge-order (CO) phenomena (lower part, with superconductive κ-salt **13** as a reference). ΔE reflects the values of the measured charge gaps for dielectric compounds; for metallic compounds, temperatures of phase transitions to insulator (T_{MI}) or superconductive (T_c) state are listed. The compounds are arranged in descending order of the thickness of the anionic (insulating) layer.

Compound Name	w^{An}	w^{Cat}	*sep* [1]	*pntr*	ΔE (meV)	Refs.
(**2**) α-(BEDT-TTF)$_{10}$(18-crown-6)$_6$K$_6$[Fe(C_2O_4)$_3$]$_4$(H_2O)$_{24}$	17.2	16.2	15.7	1.4	105	[71]
(**1**) κ_2-(BEDT-TTF)$_2$$K^+$(18-crown-6)[$Co^{II}(NCS)_4$]·($H_2O$)	13.7	16.2	11.8	1.9	570	[2]
(**3**) β''-(BEDT-TTF)$_2$[(H_2O)(NH_4)$_2$M(C_2O_4)$_3$]·18-crown-6 [3]	12.7	14.7	12.5	0.2	(T_c 2.7, 1.8 K)	[72–74]
(**4a**) α'''-(BEDT-TTF)$_9$[Cr(C_2O_4)$_3$]$_8$$Na_{18}$($H_2O$)$_{24}$	10.6	13.9	12.3	−1.7	66	[75]
(**4b**) α'''-(BEDT-TTF)$_9$[Fe(C_2O_4)$_3$]$_8$$Na_{18}$($H_2O$)$_{24}$	10.6	13.9	12.3	−1.7	77	[71]
(**5**) β''-(BEDT-TTF)$_4$[(H_3O)M(C_2O_4)$_3$]$_2$[(H_3O)$_2$(18-crown-6)]·5H_2O [4]	9.7	14.6	9.5	0.2	(T_{MI} 190, 240 K)	[76,77]
(**6**) α_2-(BEDT-TTF)$_8$[PNi(H_2O)$W_{11}O_{39}$]·2H_2O	7.5	16.4	5.3	2.2	100–150	[78]
(**7**) β''-(BEDT-TTF)$_4$$Re_6Se_5Cl_9$·[guest] [5]	6.2	14.1	4.0	2.2	(T_{MI} 50, 90 K)	[79]
(**8**) κ_2-(BEDT-TTF)$_4$[M(CN)$_6$][$N(C_2H_5)_4$]·2H_2O [6]	5.0	16.1	3.1	1.8	281	[50]
(**9**) κ_1-(BEDT-TTF)$_2$B(CN)$_4$	4.4	15.3	2.6	1.8	140	[80]
(**10**) κ_1-(BEDT-TTF)$_4$[$OsNOCl_5$]·C_6H_5CN	4.1	15.1	2.1	2.0	100	[81]
(**11**) κ_1-(BEDT-TTF)$_2$$TaF_6$	3.3	15.8	1.5	1.8	120	[82]
(**12**) κ_1-(BEDT-TTF)$_2$Hg(SCN)$_2$Cl	3.3	15.8	2.3	1.0	(T_{MI} 30 K)	[56]
(**13**) κ-(BEDT-TTF)$_2$Cu[$N(CN)_2$]Br	0	12.4	2.4	−2.4	(T_c 12 K)	[10]

[1] see Appendix A; [2] this work; [3] M = Rh, Cr, Ru, Ir; [4] M = Cr, Ga; [5] guest = DMF, THF, dioxane; [6] M = Co, Fe.

It seems to be a plausible approach using 18-crown-6 for the expansion of the interlayer dimension by increasing the anion layer thickness. It is widely believed that separation between conducting layers is a key parameter that has to be adjusted to increase the maximum value of superconductive critical temperature (T_c), which stagnates for decades [83]. The highest ambient pressure T_c for organic superconductors T_c = 12 K (**13**) has remained unsurpassed since 1990 [10]. However, the presence of crown ether in the reaction media does not guarantee inclusion of crown ether into the composition of the anion layers (in fact, the inclusion is rarely observed).

The geometries of ***A*** and ***B*** differ considerably. In radical cation ***A*** atoms C1–C6 and S1–S4 of inner tetrathiafulvalene (TTF) core and four peripheral sulfur atoms S5–S8 that are involved into intramolecular electron exchange are nearly planar that is a usual case for partially or fully charged ET radical cation (Figures 3 and 4). However, in a neutral ET molecule, conjugation through these atoms elevates intramolecular free energy.

Separation of the TTF core atoms C11–C16 and S9–S12 and outer atoms S13–S16 in the molecule ***B*** into three almost planar tetrathiaethylene (TTE) fragments brakes through the conjugation system, lowering molecular free energy. The interplanar angles between TTE parts that characterize molecular bending constitute are 21.32° and 14.02°, which exceed the values found in the structure of neutral ET donor, giving 13.4° and 12.1° correspondingly (Figure 3) [84]. This is to be considered as an independent indication of molecule ***B*** charge neutrality.

Additionally, the ET molecular charge state can be evaluated by the bond lengths in the TTF core that are indicative of the charge degree in this family of ET (BEDT-TTF) compounds. Charge Q of the two BEDT-TTF molecules in the title salt to be calculated by the formula Q = 6.347–7.463*δ, where δ = (b + c) − (a + d), b and c are the averaged values of the C-S bond lengths, while a and d are the averaged values of the C-C bond lengths of the TTF core (Scheme 1) [85]. Conversely, each ET molecule in the dimer ***AA*** carries a charge of +1 (Q_A = 0.96(2)), and thus, a cumulative charge +2 per dimer $(ET)_2^{2+}$, while the other BEDT-TTF molecule ***B*** and the corresponding dimer ***BB*** is neutral $(ET)_2^0$ (Q_B = 0.14(3)). This suggests a full-charge separation scenario further enhanced by dimerization.

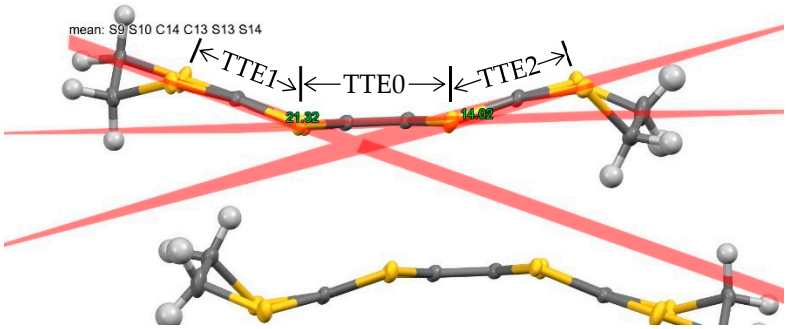

Figure 3. ***B*** molecular bending. Mean planes drawn through planar TTE parts: C11, C12, S9–S12 (TTE0, central); C13, C14, S9, S10, S13, S14 (TTE1, left); C15, C16, S11, S12, S15, S16 (TTE2, right). The legend in the upper left corner lists the atoms selected to draw the mean plane of TTE1 subunit depicted by the red semi-transparent plane drawn through the listed atoms. See Figure 4 for atom numeration.

One terminal ethylene group of ***A*** is disordered with the occupancies of 0.85/0.15 (Figure 4e). A peculiarity of this disorder is that not only are the terminal ethylene groups disordered, but so are the sulfur atoms that bear the ethylene group. Disordering parts other than terminal ethylene group is rare but not unique case for ET salts and related compounds. For example, in the salt β-$(DOET)_4CuBr_4$·PhCl, the entire annealed dioxane ring is disordered (DOET is acronym of (1,4-dioxanediyl-2,3-dithio)ethylene-dithiotetrathiafulvalene, formed by replacing one of the ET terminal ethylene group with 1,4-dioxane ring) [86].

Overlapping of planar parts of ET radical cations inside the dimers ***AA*** and ***BB*** is essentially the same. Inside dimers ***AA*** radical cations ***A*** are displaced longitudinally by a length of central BEDT-TTF C=C bond. The displacement inside dimers ***BB*** is just slightly larger with the additional tiny shift along the molecular short axis (Figure 4a,c).

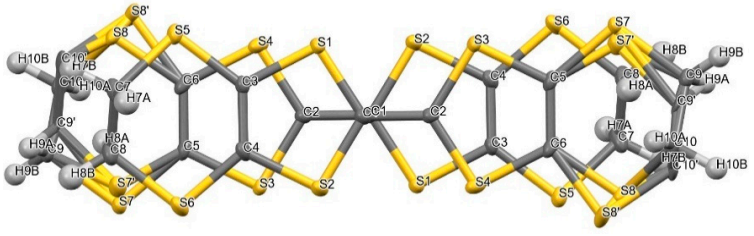

(**a**)

Figure 4. *Cont.*

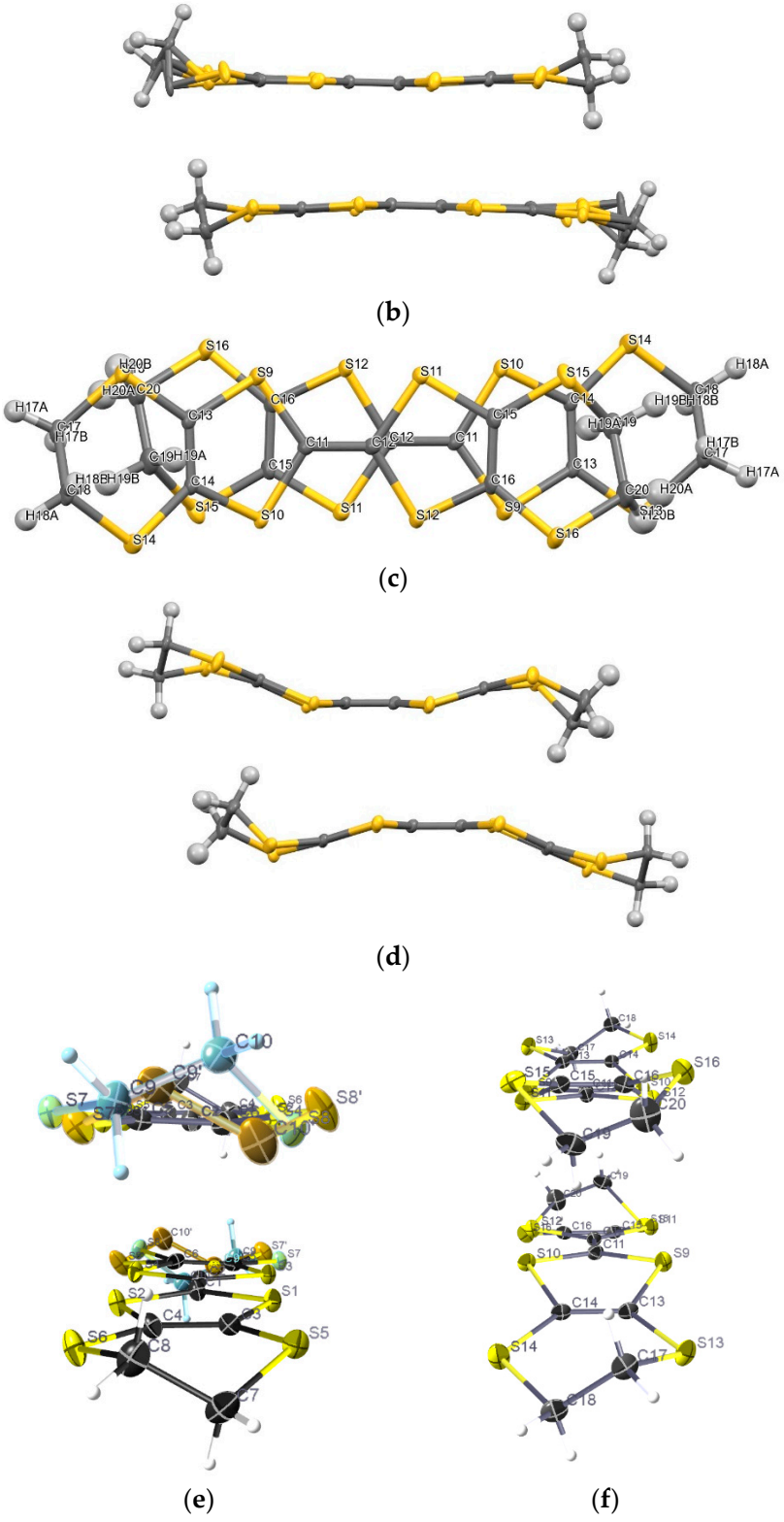

Figure 4. Atom numbering scheme for unique organic molecules ***A*** and ***B*** and intradimer arrangement for dimers ***AA*** and ***BB*** in the salt **1**. Disordered atoms are numbered by a prime scheme—C9′, C10′, S7′, S8′. Occupancies are 0.85/0.15. (**a**) Dimer ***AA***, top view; (**b**) Dimer ***AA***, side view; (**c**) Dimer ***BB***, top view; (**d**) Dimer ***BB***, side view; (**e**) Dimer ***AA***, long-through view, ellipsoids probability 50%; (**f**) Dimer ***BB***, long-through view, ellipsoids probability 50%.

Within the conductive layers, centrosymmetrical dimers ***AA*** and ***BB*** are organized into [***AA-AA-AA-***]$_\infty$ and [***BB-BB-BB-***]$_\infty$ ladder-like chains expanding along the ***a*** axis, where the mean planes of incorporated ET molecules are parallel. This segregation is not recognizable in a common projection presented in the Figure 1b. However, side views of ***AA-AA*** and ***BB-BB*** chains provide irrefutable evidence of markedly different geometry of the chains ***AA*** and ***BB*** (Figure 5).

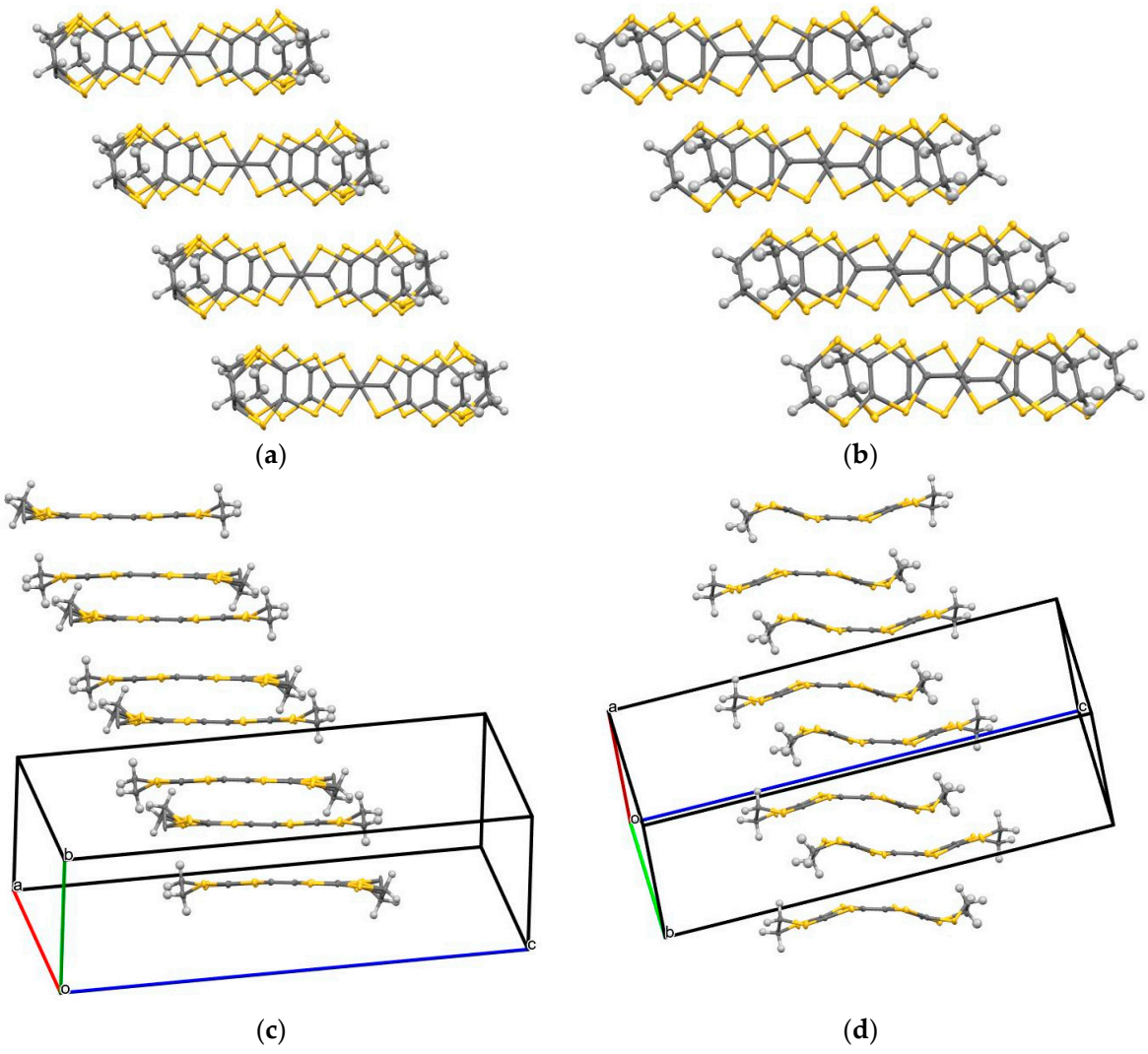

Figure 5. (**a**) ***AA-AA*** chain. Top view; (**b**) ***BB-BB*** chain. Top view; (**c**) ***AA-AA*** chain. Side view; (**d**) ***BB-BB*** chain. Side view.

The mutual arrangement of BEDT-TTF radical cations and their dimers in conductive layers is of paramount importance for understanding the electronic properties of BEDT-TTF conductive salts, which are essentially two-dimensional (2D) in nature [5]. The widely accepted rational nomenclature of ET salts refers only to the projection of the conductive layers along the ET molecular long axis (Figure 2b) [3]. The nomenclature normally grasps the electronic property essentials of the materials under investigation.

However, in some particular cases, it is necessary to consider the longitudinal displacements of ET radical cations, which are imperceptible in the aforementioned projection. Furthermore, we explore the common κ-type package in terms of "indentation" modifiers. The indents resulting from the intralayer ET radical cation longitudinal displacements naturally manifest themselves in the projections perpendicular to the one presented in Figure 2b (Figure 6).

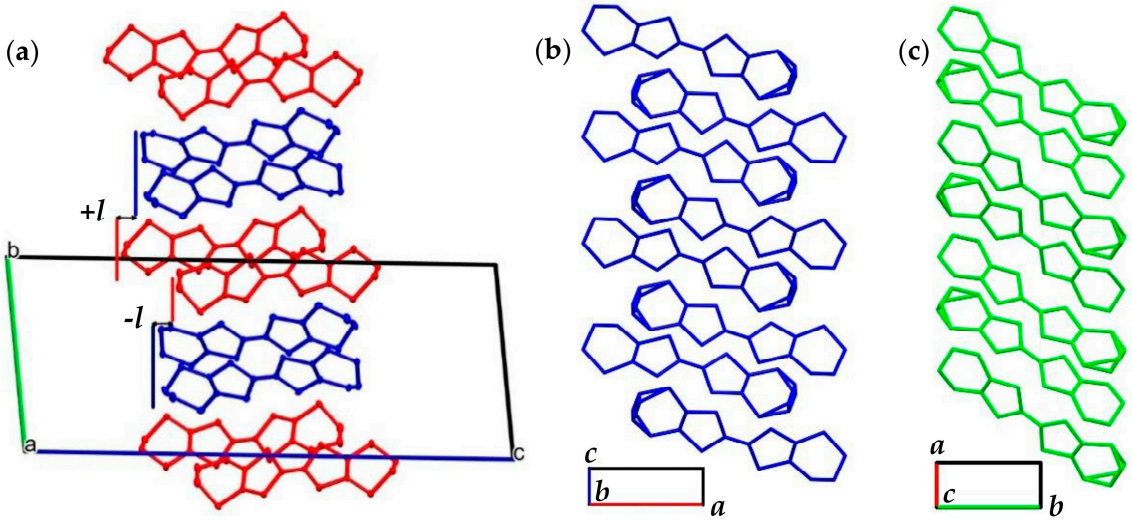

Figure 6. (**a**) Double longitudinal displacement (indent) for the conductive layer of κ_2-(BEDT-TTF)$_2$K$^+$(18-crown-6)[Co^{II}(NCS)$_4$]·(H$_2$O) (**1**) and κ_2-(BEDT-TTF)$_4$[M(CN)$_6$][N(C$_2$H$_5$)$_4$]·2H$_2$O (**8**), |l| = 1.4 Å; (**b**) Single indent for the κ_1-(BEDT-TTF)$_2$Hg(SCN)$_2$Cl (**12**), l = 2.5 Å; (**c**) Indent absence for superconductive salt κ-(BEDT-TTF)$_2$Cu[N(CN)$_2$]Br (**13**, organic layers expanding in ***ac*** plane). Structurally independent BEDT-TTF molecules are depicted by different color. See Figures S1 and S2 for salts **9**–**11**.

There is a two-step indent of 1.4 Å each (giving a cumulative indent of 2.8 Å) along the **c** dimension in the structure of organic layers expanding in ***ab*** plane (Figure 6a). This feature originates from an angular displacement (tilting) of neutral ***BB*** dimers within conductive layers. The placement of double-charged ***AA*** $(ET)_2^{2+}$ dimers inside the conductive layers repeats the arrangement that takes place in superconductive ET salts with Cu[N(CN)$_2$]X (X = Cl, Br, CN) and Cu(NCS)$_2$ anions, where no longitudinal shifts in the placements of ET dimers within the layer were observed (Figure 5c) [7,10]. The misfit of the ***BB***-chain subsystem is a consequence of the highly non-planar bent nature of molecule ***B*** that, despite similar organization of ***AA*** and ***BB*** dimers, sensibly increases effective volume and decreases symmetry of ***BB*** building block introducing extra spatial requirements for neutral ***BB*** $(ET)_2^0$ dimers.

The same double-indent feature is observed in the salt κ_2-(BEDT-TTF)$_4$[M(CN)$_6$][N(C$_2$H$_5$)$_4$]·2H$_2$O (**8**). Interestingly, the packing modes of BEDT-TTF molecules inside cation (conductive) layers look absolutely identical in salts **1** and **8**. However, anion (insulating) layers are markedly different, which breaks the otherwise possible isostructurality of salts **1** and **8** (Table 1). No other salts with the same κ-subtype were found by scrutinous analysis of the current version of the CCDC database (CSD v.5.43).

The structures of **1** and **8** were compared at T = 100 K. At this temperature, both salts demonstrate completed charge order with a positive charge located on one of two independent BEDT-TTF molecules. Structure **8** experiences phase transition around 150 K. Above 150 K in structure **8**, the charge is delocalized that is reflected by convergence of inner geometries of BEDT-TTF molecules, though ***A*** and ***B*** remain crystallographically independent [50]. That suggests to us that structure **1** is also predisposed to the same phase transition. However, taking into account the increased dielectric nature of **1** (ΔE = 570 meV in **1** vs. 281 meV in **8**, where ΔE is a width of the bandgap), the phase transition point of **1** is expected to be observed at temperatures higher than RT (room temperature).

Another notable example of charge-ordered κ-salt is κ_1-(BEDT-TTF)$_2$Hg(SCN)$_2$Cl (**12**). In **12**, the indented character of BEDT-TTF κ-layers also takes place. A single-indent feature with a value of 2.5 Å in **12** (Figure 6b) is considered less disruptive for smooth distribution of the Coulomb potential through conductive layers than 2.8 Å cumulative double-indent of salts **1** and **8** (Figure 6a), implying a reduced intervention of counter-charged anion layer

in **12**. The latter is reflected by a sufficiently reduced value of anion-to-cation penetration parameter (*pntr* = 1.9 Å in **1** and 1.8 Å in **8**, Table 1). Indeed, salt **12** demonstrates higher conductive properties than **1** and **8**. It is metallic down T_{MI} = 30 K, where it experiences an abrupt charge-order metal-insulator transition [56]. Below T_{MI}, strong charge fluctuations survive, which prevents charge localization on separate BEDT-TTF molecules, as in structures **1** and **8**, and hence, the appearance of pronounced structural changes in **12** [60]. Structure of **12** below 30 K, as well as above, shows only one crystallographically unique BEDT-TTF molecule that is an average of rapidly oscillating BEDT-TTF molecules with the different charge states. However, being unrecognized by a crystal structure analysis, the CO state of **12** below 30 K was rigorously confirmed by optical measurements [87].

It is important to emphasize that the aforementioned family of superconductive κ-salts, including κ-(BEDT-TTF)$_2$Cu[N(CN)$_2$]Br (**13**) with the highest up to date T_c = 12 K for molecular conductors at ambient pressure, have no indents in layered structure of conductive BEDT-TTF κ-layers (Figure 5c). This uniformity is probably a requirement for a smooth distribution of Coulomb potential casting by anions that prevents Cooper pair breaking, saving the superconductive state. Analysis of the data presented in Table 1 allows us to conclude that the increase of the conductive properties in the row **1** < **12** < **13** directly correlates with the decrease of the BEDT-TTF layer thickness ($w^{\mathbf{Cat}}$) 16.2 Å > 15.8 Å > 12.4 Å (Table 1). The row reflects the fact that the sparse ET layers in **1** become significantly denser in **13**, taking an intermediate value in single-indent salt **12** and other single indented salts **9**–**12**. The values for indented salts are close one another while the value for non-indented salt **13** is remarkably smaller. The latter can be speculated as the extremal (no κ BEDT-TTF salts with smaller $w^{\mathbf{Cat}}$ value were found in CCDC database) and, probably, optimal value.

Based on the aforementioned observations, we propose to update the rational nomenclature of ET κ-salts using subscripts reflecting the number of indents. Two additional subtypes κ_1- and κ_2- were recognized inside the parent κ-type. Table 1 has already been updated with this scheme. We propose to keep the symbol for the unindented (κ_0 in this numeration) as unmodified—namely, κ (see Supporting Information Figures S1 and S2 for a graphical representation of the indentation of salts **9**–**11**, listed in Table 1).

It is useful to summarize some general tendencies and key parameters playing an important role in the realization of high conductivity or superconductivity, which manifested in the data of Table 1:

1. Small value of conductive cation layer thickness—$w^{\mathbf{Cat}}$. The lower the value, the denser the conductive layer and the stronger intermolecular integrals. This provides effective intermolecular electron transfer, increasing intralayer carrier mobility. Otherwise, a sparse ET-layer structure reflects presence of indents and other inhomogeneities, hindering free carrier mobility.
2. A small value of anion-to-cation penetration coefficient—*pntr*. This obviously decrease the Coulomb disturbance of radical cation conductive layers by negative potential field of the anion layer.
3. However, the interplay of charge uniformity and charge separation within conductive layers remains the major factor that rules the conductive properties of ET salts. Thus, a full charge separation scenario realized in salts **1** and **8** predetermines their semiconductive properties, whereas superconductive salt **13** is characterized by even distribution of charge over conductive ET layers. This marked difference in conductive properties takes place despite the fact that all aforementioned salts retain a κ-type arrangement of conductive ET layers, which generally favors high conductivity.

As will be seen in the next section, the majority of the transfer integrals are within the chains with only minor connectivity between the chains. This is to be interpreted as an essentially quasi-one-dimensional (q1D) nature of charge transport in salt **1**. This is in a marked contrast with the aforementioned superconductive κ(kappa)-salts (e.g., **13**), where conductive layers are highly isotropic, which leads to a quasi-two-dimensional (q2D) electronic structure.

3.2. Electronic Structure

The electronic band structure calculated by means of the extended Hückel tight-binding (EHTB) approach is a convenient and straightforward way to gain some insight into the relationship between crystal structure and transport properties. The results of the calculations for salt **1** based on the crystal structure geometry, neglecting electron–electron correlations, are summarized in Figures 7 and 8 and Table 2.

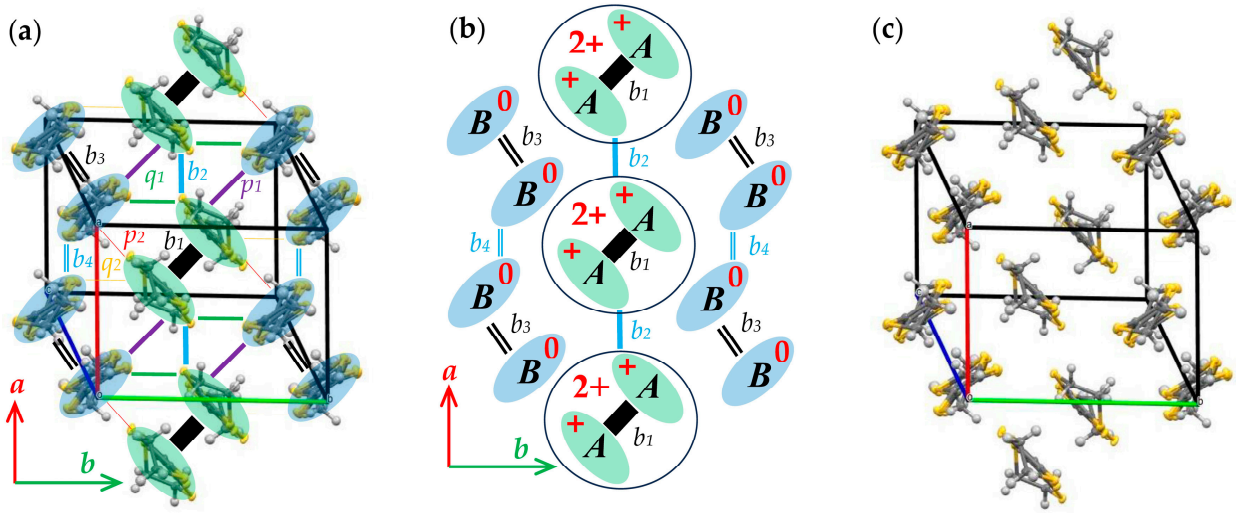

Figure 7. (**a**) Transfer integrals (TI) network in salt **1** for single conductive organic ET layer in the projection along long molecular axis of ET (ab plane). The line thicknesses reflect the TI values, while colors reflect the TI symmetry. The lines for TI between neutral ET molecules (***B-B*** type) are dignified with double strokes. The corresponding values of the TI are listed in Table 2. (**b**) Selected superstripe bounded by two adjacent chains built from neutral ET dimers. Positively charged dimers are selected by circles. Charges are shown by numbers and '+' sign. For clarity, only in-chain TI are shown. (**c**) Fragment of the conductive layer projected along the ET long axis within the ***ab*** plane.

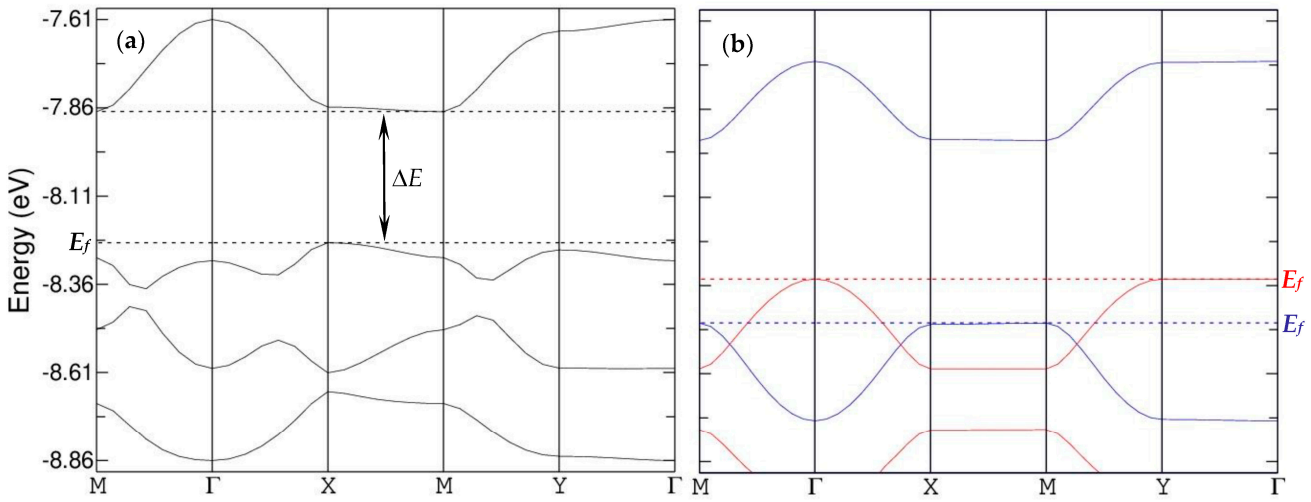

Figure 8. (**a**) The Fermi energy (E_f = −8.25 eV) level is depicted by the lower horizontal dashed line. Upper dashed line represents the bottom of the lowest empty zone. Coulomb bandgap ΔE = 0.37 eV is shown by the double-headed arrow. (**b**) Band structure of the chains ***AA*** (positive, blue) and ***BB*** (neutral, red) calculated independently from each other prior to the hybridization.

Table 2. The transfer integrals between BEDT-TTF molecules in salt **1**.

Transfer Integral	Energy (meV)
b_1	622.5
b_2	174.3
b_3	−301.6
b_4	160.8
p_1	−157.4
p_2	2.9
q_1	−115
q_2	−8.6

It can be immediately seen from Table 2 that the major effect is a very strong dimerization of positively charged radical cations ***A*** (transfer integrals b_1). Secondarily, double-charged ***AA*** units are compiled into chains by the strongest inter-dimer transfer integrals b_2. Similarly, with lower energies of the transfer integrals involved, neutral ***BB***-chains are organized. Taken independently, ***BB***-chains hardly provide reasonable pathway for carrier transport, even implying activation mechanism. That is a direct consequence of charge neutrality of the incorporated ET-units and, hence, very large energy gap between upper occupied and lower empty intrachain bands. The adjacent ***AA***- and ***BB***-chains are coupled mainly by p_1 and q_1 integrals with near-zero p_2 and q_2 integrals (Table 2, Figure 7). These observations reveal a square lattice for salt **1**.

Band structure demonstrates medium-to-low dispersion along axis ***b*** (Figure 8a). This is in the contrast with the very high dispersion along axis ***a***. Band structure of chains ***AA*** and ***BB*** taken independently provides qualitatively similar picture (Figure 8b). One should keep in mind that the lowest empty band for neutral ***BB***-chains is formed from BEDT-TTF LUMO levels, and subsequently, lies far above the picture energy scale. Conversely, the lowest empty band for charged ***AA***-chains is formed from BEDT-TTF HOMO levels, and thus, it is accessible for activation transport. The main effect of the hybridization of upper occupied bands of ***AA***- and ***BB***-chains is raising of the Fermi level, which in turn reduces activation energy ΔE. This indicates relatively low coupling of ***AA***- and ***BB***- chains in the square lattice and axis ***a*** as a preferrable direction for current flow, imposing presumably q1D conduction architecture.

This arrangement is reminiscent of the horizontal charge order stripes found in the charge-ordered θ-ET salts (e.g., θ-$ET_2RbCo(SCN)_4$) [46]; however, in this particular case, vertical charge-order stripes are formed. The difference between horizontal and vertical stripe orders is in the symmetry of transfer integrals driven by the interplane angle between adjacent ET-s in the chain. The mean planes of incorporated ET-s are inclined (for simplicity—orthogonal) in the former and parallel in the latter [35,47]. Assuming an enhanced level of charge separation in salt **1**, comparing with θ-salts, the chains of BEDT-TTF ***AA*** dimers with the charge +2 running along axis ***a*** are named superstripes in the current work. The resulted spatial pattern of charge ordering is a stripe alternating along axis ***b***.

The band structure proposes an activation transport, where the carriers are injected from the fully occupied upper band of ***BB***-chains to the empty upper band of ***AA***-superstripes. The calculated value of the charge gap is 0.37 eV (Figure 8). This is about 1/3rd below (0.57 eV, see next section) the measured value. Usually, EHTB calculations tend to overestimate the actual gap value as a real structure with actual imperfections/inclusions providing doping centers and carrier shortways is not taken into account [88]. However, in this particular case, underestimation of the gap value serves as a sign of the presence of persisting electronic correlations that often lead to opening of the Mott gap in formally 3/4th filled upper band for ET compounds with +0.5 charge per ET radical cation [89].

3.3. Electrical Resistivity

Curve for normalized in-plane resistance measured along axis ***a*** (direction of maximum conductivity) of salt **1** is presented in Figure 9. The salt demonstrates semicon-

ductive type of R(*T*) dependence from ambient temperature (297 K) down to measured temperatures. Room temperature resistivity is 3 Ω·cm that is a usual value for semiconductive ET salts with formal +0.5 charge per BEDT-TTF radical cation (e.g., recent δ_0-(BEDT-TTF)$_2$(TaF$_6$)$_{0.43}$(PF$_6$)$_{0.57}$ has ρ = 2–6 Ω·cm [90], and α′-(BEDT-TTF)$_2$[Cr(C$_2$O$_4$)$_2$(2,2′-bipy)]·CHCl$_2$CH$_2$Cl has ρ = 2 Ω·cm [91]). However, the measured value for the charge gap retrieved from fitting the linear part of the Arrhenius plot was 0.57 eV (Figure 9, inset). This high value of the charge gap is characteristic of BEDT-TTF conductive salts containing only single-charged (BEDT-TTF)$^+$ radical cations (e.g., β-(BEDT-TTF)TaF$_6$ has ΔE = 0.55 eV [92]).

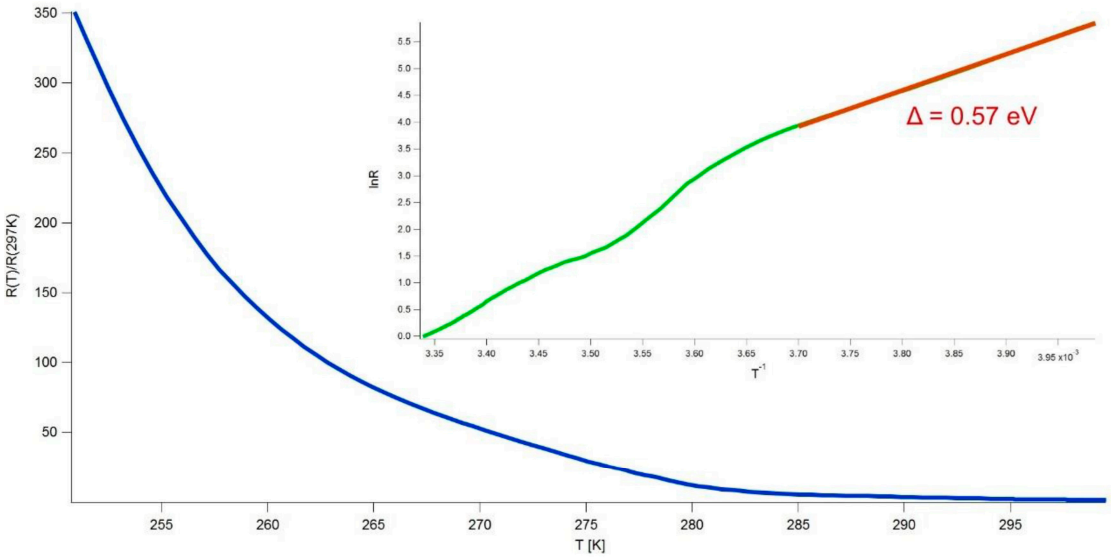

Figure 9. Temperature dependence of the normalized electrical resistance for salt **1** along axis ***a***. (**inset**) Arrhenius plot in natural logarithm coordinates of normalized electrical resistance (lnR) vs. reciprocal temperature (T^{-1}). Linear part for the fitting is depicted by red color.

The formal charge in salt **1** is +0.5 per BEDT-TTF molecule that implies a quarter- or half-filled upper band and metallic type conductivity if neglecting electron-electron (***e-e***) correlations. However, in salt **1**, full charge segregation between two crystallographically unique molecules ***A*** and ***B*** as well as spatial separation of charged +1 (***A***) and neutral (***B***) BEDT-TTF-s provides crystal and electronic structures more resembling cases of salts where only single-charged organic donor radical cations are presented (see above). The latter also possess fully occupied upper band and demonstrate activated type conductivity with the Coulomb energy gap [92].

4. Conclusions

Single crystals of conductive charge-transfer radical cation salt κ_1-(BEDT-TTF)$_2$Co^{II}(NCS)$_4$[K$^+$(18-crown-6)] (**1**) possessing magnetic Co^{II} centers was synthesized by means of anodic electrooxidation of BEDT-TTF in solution. Its crystal, electronic, and band structures as well as electrical conductivity have been thoroughly examined.

The thickness of anionic insulating layers of salt **1** is almost a record among all reported BEDT-TTF layered salts owing to the unique pancake-like four-decker architecture. Two inner sublayers of K$^+$ monocations coordinated by bulky crown ether 18-crown-6 are canted by two outer sublayers of dianion Co(SCN)$_4^{2-}$. Due to the elevated anion layer (insulating) thickness, effective separation of radical cation (conductive) layers reaches a value of 11.8 Å.

Radical cation layers responsible for conductivity are built by κ-type, where two crystallographically unique ET molecules ***A***, charged positively, and ***B***, neutral, form face-to-face dimers $\boldsymbol{AA}^{2+}$ and $\boldsymbol{BB}^0$ arranged in a checkerboard pattern. Crystallographically independent ET-s are markedly distinct not only by intramolecular bond lengths but also

by conformation. Positively charged ET^+ radical cation ***A*** is flat, while neutral molecule ***B*** is bent.

A new type of charge ordering (CO) pattern, i.e., vertical superstripes, has been detected: strongly dimerized single-charged ET radical cations $(ET)_2^{2+}$ (***AA***) are regarded as single units forming a stepwise chain running along axis ***a*** in the manner when plain parts of all incorporated ETs are parallel. Positively charged chains are alternating along axis ***b*** with neutral ones composed from $(ET)_2^0$ (***BB***) dimeric units. The suffix super stands for a duplication of charge located on the repeating single unit of the chain and subsequent enhancement of all effects concerning charge ordering.

The ground state of salt **1** is the interdimer CO state. Transfer integrals for ***AA*** dimers are far stronger than the others. In turn, ***AA*** dimers are combed in superstripes by the strongest out-of-dimer transfer integrals. Moderately coupled superstripes form a square lattice. However, by the sum of factors, its electronic dimensionality is closer to q1D than q2D.

EHTB calculations indicate full band separation with a Coulomb gap value of 0.75 eV. It overestimates the measured value of 0.57 eV by about 30%, which is consistent with EHTB intrinsic limitations. This high value of measured charge gap is reminiscent of salts containing single charged ET^+ only, rather than the salts with a +0.5 ET formula charge.

In the current report, we update the rational nomenclature for ET κ-salts, which regards mainly the 2D projection of the conductive layer along the long axis of ET, by thorough analysis of mutual arrangements and repeating motifs of ET radical cations in the dimension that is perpendicular to the layer expansion one. Two additional subtypes κ_1- and κ_2- were recognized inside the parent κ-type, where subscripts denote the quantity of indents modifying ET layers in the perpendicular dimension. The symbol for the unindented (κ_0 in this numeration) layer is left unmodified—κ. Salt **1** belongs to the κ_2-type.

Indentation is directly connected to the conductivity. Thus, unindented κ-$ET_2Cu[N(CN)_2]Br$ is a superconductor with the highest T_c = 12 K among radical cation salts at ambient pressure. Moreover, κ_1-$ET_2Hg(SCN)_2Cl$ is a metal down to 30 K, where it experiences MI transition, which, however, is easily suppressed by the application of a moderate hydrostatic pressure of 0.7 kbar [58].

Although conductive ET κ-layers of salt **1** is a replica of that for salt κ_2-$(BEDT\text{-}TTF)_4[M(CN)_6][N(C_2H_5)_4]\cdot 2H_2O$ (**8**), no semi-metallic part was observed on the resistivity curve, and it is insulating down from ambient temperature, semi-metallic or metallic behavior could be observable at elevated temperatures. High temperature measurements are planned for the future.

Supplementary Materials: The following supporting information can be downloaded at: https://www.mdpi.com/article/10.3390/cryst13101504/s1, Figure S1: Side projection of radical cation (conductive) layers of salts **9**–**11** visualizing indents modifying ET layers in the direction that is perpendicular to the direction of layer expansion [S1–S3] (or [93–95] in the main list). New annotation scheme—κ_N, where N is the number of indents applied. Different colors denote unequivalent molecules. Hydrogens are hidden for clarity. Figure S2: Side view of the radical cation (conductive) layers of salts **9** and **11** with uncut cell vectors.

Author Contributions: Conceptualization, data curation, manuscript preparation, X-ray diffraction and structural analysis, and calculation of transfer integrals and band structure, A.A.B.; electrocrystallization, T.G.P.; resistivity measurements, L.I.B. All authors have read and agreed to the published version of the manuscript.

Funding: The work was supported by the Ministry of Science and Higher Education of the Russian Federation (grant No. 075-15-2020-779).

Data Availability Statement: Crystallographic supplementary data (.cif files) can be received at no charge from the website https://www.ccdc.cam.ac.uk/structures/ (accessed on 1 October 2023). Additional experimental and computational data are available from the corresponding author upon reasonable request.

Acknowledgments: The authors are grateful to E. B. Yagubskii for fruitful discussions and thorough support and to G. V. Shilov for assistance in X-ray data collection.

Conflicts of Interest: The authors declare no conflict of interest.

Appendix A

The definitions of the new terms introduced in Table 1 are as follows:
w^{An} = thickness (width) of the anion layer;
w^{Cat} = thickness (width) of the radical cation layer;
sep = separation between cation layers;
pntr = interpenetration of anion and cation layers.

Thickness (width) of the anion or cation layer (w^{An}/w^{Cat}) is defined as a difference in coordinates along the layer separation axis between the most distant atoms along the axis. For salt **1**, the layer separation axis is ***c***, its value constituting 28.21 Å. The most distant atoms for the anion (insulating) layer are S2A and S2A($1-x$, $1-y$, $-z$), with the coordinate difference in Angstroms as follows:

$$w^{An}(\mathbf{1}) = (0.244179 - -0.244179) \times 28.21 = 13.776 \text{ Å}.$$

The most distant atoms for the cation (conductive) layer are H18A and H18A($1-x$, $1-y$, $1-z$), with the coordinate difference in Angstroms as follows:

$$w^{Cat}(\mathbf{1}) = (0.789662 - 0.210338) \times 28.21 = 16.343 \text{ Å}.$$

Separation between cation layers (*sep*) is taken as a difference between length of the layer separation axis and thickness (width) of the radical cation layer (w^{Cat}):

$$sep = \boldsymbol{c} - w^{Cat}.$$

For the salt **1**:

$$sep(\mathbf{1}) = 28.21 - 16.343 = 11.867 \text{ Å}.$$

Interpenetration of the anion and cation layers (*pntr*) is taken as the difference between the sum of layers widths and length of the layer separation axis:

$$pntr = w^{An} + w^{Cat} - \boldsymbol{c}.$$

For the salt **1**:

$$pntr(\mathbf{1}) = 13.776 + 16.343 - 28.21 = 1.909 \text{ Å}.$$

Note that a smooth conductive layer without indents and a single-atom thick anion layer, as in the case of salt **13**, does not imply a zero *pntr* parameter. Rather, it takes negative values (Table 1). There is a hidden parameter Δ associated with non-covalent interactions between the anion and cation layers that is not taken into account in the current calculations. The full formula for the repeating unit reads:

$$\boldsymbol{c} = w^{An} + w^{Cat} - pntr = w^{An} + w^{Cat} - pntr^0 + \Delta$$

where $pntr_0 = pntr + \Delta$ is a refined penetration coefficient, which is always non-negative. Assuming $pntr_0$ takes a zero value in the case of salt **13**, we approximate that the coefficient Δ is circa 2.4 Å in the case of κ-salts. It is quite natural to consider the table value *pntr* for salt **13** as a natural minimum for κ-salts (Table 1).

References

1. Zhu, Y.Y.; Liu, F.; Liu, J.J.; Meng, Y.S.; Jiang, S.D.; Barra, A.L.; Wernsdorfer, W.; Gao, S. Slow Magnetic Relaxation in Weak Easy-Plane Anisotropy: The Case of a Combined Magnetic and HFEPR Study. *Inorg. Chem.* **2017**, *56*, 697–700. [CrossRef] [PubMed]
2. Mori, T. Structural Genealogy of BEDT-TTF-Based Organic Conductors I. Parallel Molecules: β and β″ Phases. *Bull. Chem. Soc. Jpn.* **2006**, *71*, 2509–2526. [CrossRef]
3. Mori, T.; Mori, H.; Tanaka, S. Structural Genealogy of BEDT-TTF-Based Organic Conductors II. Inclined Molecules: θ, α, and κ Phases. *Bull. Chem. Soc. Jpn.* **2003**, *72*, 179–197. [CrossRef]
4. Mori, T. Structural Genealogy of BEDT-TTF-Based Organic Conductors III. Twisted Molecules: δ and α′ Phases. *Bull. Chem. Soc. Jpn.* **2004**, *72*, 2011–2027. [CrossRef]
5. Fukuyama, H. Physics of Molecular Conductors. *J. Phys. Soc. Jpn.* **2006**, *75*, 051001. [CrossRef]
6. Bardin, A.A.; Akutsu, H.; Yamada, J.-I. New Family of Six Stable Metals with a Nearly Isotropic Triangular Lattice of Organic Radical Cations and Diluted Paramagnetic System of Anions: κ(κ$_\perp$)-(BDH-TTP)$_4$MX$_4$·Solv, Where M = Co^{II}, Mn^{II}; X = Cl, Br, and Solv = $(H_2O)_5$, (CH_2X_2). *Cryst. Growth Des.* **2016**, *16*, 1228–1246. [CrossRef]
7. Urayama, H.; Yamochi, H.; Saito, G.; Nozawa, K.; Sugano, T.; Kinoshita, M.; Sato, S.; Oshima, K.; Kawamoto, A.; Tanaka, J. A New Ambient Pressure Organic Superconductor Based on BEDT-TTF with T_C Higher than 10 K (T_C = 10.4 K). *Chem. Lett.* **1988**, *17*, 55–58. [CrossRef]
8. Bardin, A.A.; Burn, P.L.; Lo, S.C.; Powell, B.J. Superconductivity Suppression and Peak Resistivity Enhancement for Thin Crystals of κ-(BEDT-TTF)$_2$Cu(SCN)$_2$. *Phys. Stat. Solidi B* **2012**, *249*, 979–984. [CrossRef]
9. Kawaguchi, G.; Bardin, A.A.; Suda, M.; Uruichi, M.; Yamamoto, H.M. An Ambipolar Superconducting Field-Effect Transistor Operating above Liquid Helium Temperature. *Adv. Mater.* **2019**, *31*, 1805715. [CrossRef]
10. Kini, A.M.; Geiser, U.; Wang, H.H.; Carlson, K.D.; Williams, J.M.; Kwok, W.K.; Vandervoort, K.G.; Thompson, J.E.; Stupka, D.L.; Jung, D.; et al. A New Ambient-Pressure Organic Superconductor, κ-(ET)$_2$Cu[N(CN)$_2$]Br, with the Highest Transition Temperature Yet Observed (Inductive Onset Tc = 11.6 K, Resistive Onset = 12.5 K). *Inorg. Chem.* **1990**, *29*, 2555–2557. [CrossRef]
11. Milbradt, S.; Bardin, A.A.; Truncik, C.J.S.; Huttema, W.A.; Jacko, A.C.; Burn, P.L.; Lo, S.-C.; Powell, B.J.; Broun, D.M. In-Plane Superfluid Density and Microwave Conductivity of the Organic Superconductor κ-(BEDT-TTF)$_2$Cu[N(CN)$_2$]Br: Evidence for *d*-Wave Pairing and Resilient Quasiparticles. *Phys. Rev. B* **2013**, *88*, 064501. [CrossRef]
12. Guterding, D.; Altmeyer, M.; Jeschke, H.O.; Valentí, R. Near-Degeneracy of Extended $s + d_{x^2-y^2}$ and d_{xy} Order Parameters in Quasi-Two-Dimensional Organic Superconductors. *Phys. Rev. B* **2016**, *94*, 024515. [CrossRef]
13. Wosnitza, J. Superconductivity of Organic Charge-Transfer Salts. *J. Low Temp. Phys.* **2019**, *197*, 250–271. [CrossRef]
14. Shevchun, A.F.; Bardin, A.A.; Kotov, A.I.; Shovkun, D.V. Peculiarities of the Transport Properties of a Strongly Correlated Incommensurate Organic Superconductor κ-(BEDT-TTF)$_4$Hg$_{2.89}$Br$_8$. *J. Surf. Investig.* **2021**, *15*, 1286–1289. [CrossRef]
15. Shimizu, Y.; Miyagawa, K.; Kanoda, K.; Maesato, M.; Saito, G. Spin Liquid State in an Organic Mott Insulator with a Triangular Lattice. *Phys. Rev. Lett.* **2003**, *91*, 107001. [CrossRef]
16. Powell, B.J.; McKenzie, R.H. Quantum Frustration in Organic Mott Insulators: From Spin Liquids to Unconventional Superconductors. *Rep. Prog. Phys.* **2011**, *74*, 056501. [CrossRef]
17. Riedl, K.; Valentí, R.; Winter, S.M. Critical Spin Liquid versus Valence-Bond Glass in a Triangular-Lattice Organic Antiferromagnet. *Nat. Commun.* **2019**, *10*, 2561. [CrossRef]
18. Pustogow, A. Thirty-Year Anniversary of κ-(BEDT-TTF)$_2$Cu$_2$(CN)$_3$: Reconciling the Spin Gap in a Spin-Liquid Candidate. *Solids* **2022**, *3*, 93–110. [CrossRef]
19. Miksch, B.; Pustogow, A.; Rahim, M.J.; Bardin, A.A.; Kanoda, K.; Schlueter, J.A.; Hübner, R.; Scheffler, M.; Dressel, M. Gapped Magnetic Ground State in Quantum Spin Liquid Candidate κ-(BEDT-TTF)$_2$Cu$_2$(CN)$_3$. *Science* **2021**, *372*, 276–279. [CrossRef]
20. Saito, Y.; Löhle, A.; Kawamoto, A.; Pustogow, A.; Dressel, M. Pressure-Tuned Superconducting Dome in Chemically-Substituted κ-(BEDT-TTF)$_2$Cu$_2$(CN)$_3$. *Crystals* **2021**, *11*, 817. [CrossRef]
21. Yamada, J.-i.; Watanabe, M.; Anzai, H.; Nishikawa, H.; Ikemoto, I.; Kikuchi, K. BDH-TTP as a Structural Isomer of BEDT-TTF, and Its Two-Dimensional Hexafluorophosphate Salt. *Angew. Chem. Int. Ed.* **1999**, *38*, 810–813. [CrossRef]
22. Huddart, B.M.; Lancaster, T.; Blundell, S.J.; Guguchia, Z.; Taniguchi, H.; Clark, S.J.; Pratt, F.L. μSR Investigation of Magnetism in κ-(ET)$_2$X: Antiferromagnetism. *Phys. Rev. Res.* **2023**, *5*, 013015. [CrossRef]
23. Kanoda, K. Recent Progress in NMR Studies on Organic Conductors. *Hyperfine Interact.* **1997**, *104*, 235–249. [CrossRef]
24. Dressel, M. Quantum Criticality in Organic Conductors? Fermi Liquid versus Non-Fermi-Liquid. *J. Phys. Condens. Matter* **2011**, *23*, 293201. [CrossRef]
25. Tomić, S.; Dressel, M. Ferroelectricity in Molecular Solids: A Review of Electrodynamic Properties. *Rep. Prog. Phys.* **2015**, *78*, 096501. [CrossRef]
26. Dressel, M.; Tomić, S. Molecular Quantum Materials: Electronic Phases and Charge Dynamics in Two-Dimensional Organic Solids. *Adv. Phys.* **2020**, *69*, 1–120. [CrossRef]
27. Kagawa, F.; Miyagawa, K.; Kanoda, K. Magnetic Mott Criticality in a κ-Type Organic Salt Probed by NMR. *Nat. Phys.* **2009**, *5*, 880–884. [CrossRef]
28. Furukawa, T.; Miyagawa, K.; Taniguchi, H.; Kato, R.; Kanoda, K. Quantum Criticality of Mott Transition in Organic Materials. *Nat. Phys.* **2015**, *11*, 221–224. [CrossRef]

29. Isono, T.; Terashima, T.; Miyagawa, K.; Kanoda, K.; Uji, S. Quantum Criticality in an Organic Spin-Liquid Insulator κ-(BEDT-TTF)$_2$Cu$_2$(CN)$_3$. *Nat. Commun.* **2016**, *7*, 13494. [CrossRef] [PubMed]
30. Gati, E.; Garst, M.; Manna, R.S.; Tutsch, U.; Wolf, B.; Bartosch, L.; Schubert, H.; Sasaki, T.; Schlueter, J.A.; Lang, M. Breakdown of Hooke's Law of Elasticity at the Mott Critical Endpoint in an Organic Conductor. *Sci. Adv.* **2016**, *2*, e1601646. [CrossRef]
31. Limelette, P.; Wzietek, P.; Florens, S.; Georges, A.; Costi, T.A.; Pasquier, C.; Jérome, D.; Mézière, C.; Batail, P. Mott Transition and Transport Crossovers in the Organic Compound κ-(BEDT-TTF)$_2$Cu[N(CN)$_2$]Cl. *Phys. Rev. Lett.* **2003**, *91*, 016401. [CrossRef] [PubMed]
32. Fournier, D.; Poirier, M.; Castonguay, M.; Truong, K.D. Mott Transition, Compressibility Divergence, and the *P-T* Phase Diagram of Layered Organic Superconductors: An Ultrasonic Investigation. *Phys. Rev. Lett.* **2003**, *90*, 4. [CrossRef]
33. Pustogow, A.; Rösslhuber, R.; Tan, Y.; Uykur, E.; Böhme, A.; Wenzel, M.; Saito, Y.; Löhle, A.; Hübner, R.; Kawamoto, A.; et al. Low-Temperature Dielectric Anomaly Arising from Electronic Phase Separation at the Mott Insulator-Metal Transition. *NPJ Quantum Mater.* **2021**, *6*, 9. [CrossRef]
34. Lunkenheimer, P.; Müller, J.; Krohns, S.; Schrettle, F.; Loidl, A.; Hartmann, B.; Rommel, R.; De Souza, M.; Hotta, C.; Schlueter, J.A.; et al. Multiferroicity in an Organic Charge-Transfer Salt That Is Suggestive of Electric-Dipole-Driven Magnetism. *Nat. Mater.* **2012**, *11*, 755–758. [CrossRef] [PubMed]
35. Seo, H.; Merino, J.; Yoshioka, H.; Ogata, M. Theoretical Aspects of Charge Ordering in Molecular Conductors. *J. Phys. Soc. Jpn.* **2006**, *75*, 051009. [CrossRef]
36. Lunkenheimer, P.; Loidl, A. Dielectric Spectroscopy on Organic Charge-Transfer Salts. *J. Phys. Condens. Matter* **2015**, *27*, 373001. [CrossRef]
37. Takahashi, T.; Nogami, Y.; Yakushi, K. Charge Ordering in Organic Conductors. *J. Phys. Soc. Jpn.* **2006**, *75*, 051008. [CrossRef]
38. Yakushi, K. Infrared and Raman Studies of Charge Ordering in Organic Conductors, BEDT-TTF Salts with Quarter-Filled Bands. *Crystals* **2012**, *2*, 1291–1346. [CrossRef]
39. Lunkenheimer, P.; Hartmann, B.; Lang, M.; Müller, J.; Schweitzer, D.; Krohns, S.; Loidl, A. Ferroelectric Properties of Charge-Ordered α-(BEDT-TTF)$_2$I$_3$. *Phys. Rev. B* **2015**, *91*, 245132. [CrossRef]
40. Satoshi, T.; Naoki, K.; Ryuhei, O.; Toshio, N.; Yasunori, T. Effects of Molecular Substitution in Organic Conductors α-(ET)$_2$I$_3$ and α-(STF)$_2$I$_3$ Studied by Polarized Femtosecond Spectroscopy. *J. Phys. Soc. Jpn.* **2023**, *92*, 094703. [CrossRef]
41. Mroweh, N.; Mézière, C.; Pop, F.; Auban-Senzier, P.; Alemany, P.; Canadell, E.; Avarvari, N. In Search of Chiral Molecular Superconductors: κ-[(S,S)-DM-BEDT-TTF]$_2$ClO$_4$ Revisited. *Adv. Mater.* **2020**, *32*, 2002811. [CrossRef] [PubMed]
42. Mori, T. Estimation of Off-Site Coulomb Integrals and Phase Diagrams of Charge Ordered States in the θ-Phase Organic Conductors. *Bull. Chem. Soc. Jpn.* **2001**, *73*, 2243–2253. [CrossRef]
43. Mori, H.; Tanaka, S.; Mori, T.; Kobayashi, A.; Kobayashi, H. Crystal Structure and Physical Properties of *M* = Rb and Tl Salts of (BEDT-TTF)$_2$*MM*′(SCN)$_4$ [*M*′ = Co, Zn]. *Bull. Chem. Soc. Jpn.* **1998**, *71*, 797–806. [CrossRef]
44. Mori, H.; Tanaka, S.; Mori, T. Systematic Study of the Electronic State in θ-Type BEDT-TTF Organic Conductors by Changing the Electronic Correlation. *Phys. Rev. B* **1998**, *57*, 12023. [CrossRef]
45. Watanabe, M.; Noda, Y.; Nogami, Y.; Mori, H. Transfer Integrals and the Spatial Pattern of Charge Ordering in θ-(BEDT-TTF)$_2$RbZn(SCN)$_4$ at 90 K. *J. Phys. Soc. Jpn.* **2004**, *73*, 116–122. [CrossRef]
46. Watanabe, M.; Noda, Y.; Nogami, Y.; Mori, H. Crystal Structure of Charge Ordered Compound θ-(BEDT-TTF)$_2$RbCo(SCN)$_4$ at Low Temperatures. *J. Phys. Soc. Jpn.* **2005**, *74*, 2011–2016. [CrossRef]
47. Seo, H. Charge Ordering in Organic ET Compounds. *J. Phys. Soc. Jpn.* **2000**, *69*, 805–820. [CrossRef]
48. Galimzyanov, A.A.; Ignat'ev, A.A.; Kushch, N.D.; Laukhin, V.N.; Makova, M.K.; Merzhanov, V.A.; Rozenberg, L.P.; Shibaeva, R.P.; Yagubskii, E.B. New Cation-Radical Salts of BEDT-TTF with the Octahedral Metal Complex Anions $PtCl_6^{2-}$, $PtBr_6^{2-}$, $TeCl_6^{2-}$ and $SnCl_6^{2-}$. Synthesis, Structure and Properties. *Synth. Met.* **1989**, *33*, 81–91. [CrossRef]
49. Doublet, M.-L.; Canadell, E.; Shibaeva, R.P. Concerning the First-Order Transition in the κ-Phase (BEDT-TTF)$_4$PtCl$_6$·C$_6$H$_5$CN. *J. Phys. I Fr.* **1994**, *4*, 1479–1490. [CrossRef]
50. Ota, A.; Ouahab, L.; Golhen, S.; Yoshida, Y.; Maesato, M.; Saito, G.; Swietlik, R. Phase Transition from Mott Insulating Phase into the Charge Ordering Phase with Molecular Deformation in Charge-Transfer Salts κ-(ET)$_4$[M(CN)$_6$][N(C$_2$H$_5$)$_4$]·2H$_2$O (M = Co^{III} and Fe^{III}). *Chem. Mater.* **2007**, *19*, 2455–2462. [CrossRef]
51. Świetlik, R.; Łapiński, A.; Połomska, M.; Ouahab, L.; Ota, A. Infrared and Raman Investigations of the Charge Ordering Phenomena in the Monoclinic Salts κ-(BEDT-TTF)$_4$[M(CN)$_6$][N(C$_2$H$_5$)$_4$]·2H$_2$O (M = Co^{III}, Fe^{III}). *J. Low Temp. Phys.* **2006**, *142*, 641–645. [CrossRef]
52. Łapiński, A.; Świetlik, R.; Ouahab, L.; Golhen, S. Spectroscopic Studies of the Phase Transition from the Mott Insulator State to the Charge-Ordering State of κ-(ET)$_4$[M(CN)$_6$][N(C$_2$H$_5$)$_4$]·2H$_2$O (M = Co^{III} and Fe^{III}) Salts. *J. Phys. Chem. A* **2013**, *117*, 5241–5250. [CrossRef] [PubMed]
53. Lyubovskaya, R.N.; Dyachenko, O.A.; Gritsenko, V.V.; Mkoyan, S.G.; Atovmyan, L.O.; Lyubovskii, R.B.; Laukhin, V.N.; Zvarykina, A.V.; Khomenko, A.G. New Organic Metal (ET)$_4$(Hg$_2$Cl$_6$·C$_6$H$_5$Cl): Synthesis, Structure, Properties. *Synth. Met.* **1991**, *42*, 1907–1910. [CrossRef]
54. Aldoshina, M.Z.; Lyubovskaya, R.N.; Konovalikhin, S.V.; Dyachenko, O.A.; Shilov, G.V.; Makova, M.K.; Lyubovskii, R.B. A New Series of ET-Based Organic Metals: Synthesis, Crystal Structure and Properties. *Synth. Met.* **1993**, *56*, 1905–1909. [CrossRef]

55. Lyubovskii, R.B.; Lyubovskaya, R.N.; Dyachenko, O.A. Physical Properties of Some ET-Based Organic Metals and Superconductors with Mercury Containing Anions. *J. Phys. I Fr.* **1996**, *6*, 1609–1630. [CrossRef]
56. Drichko, N.; Beyer, R.; Rose, E.; Dressel, M.; Schlueter, J.A.; Turunova, S.A.; Zhilyaeva, E.I.; Lyubovskaya, R.N. Metallic State and Charge-Order Metal-Insulator Transition in the Quasi-Two-Dimensional Conductor κ-(BEDT-TTF)$_2$Hg(SCN)$_2$Cl. *Phys. Rev. B* **2014**, *89*, 075133. [CrossRef]
57. Lyubovskii, R.B.; Pesotskii, S.I.; Zverev, V.N.; Zhilyaeva, E.I.; Torunova, S.A.; Lyubovskaya, R.N. Hydrostatic-Pressure-Induced Reentrance of the Metallic State in the κ-(ET)$_2$Hg(SCN)$_2$Cl Quasi-Two-Dimensional Organic Conductor. *JETP Lett.* **2020**, *112*, 582–584. [CrossRef]
58. Ivek, T.; Beyer, R.; Badalov, S.; Čulo, M.; Tomić, S.; Schlueter, J.A.; Zhilyaeva, E.I.; Lyubovskaya, R.N.; Dressel, M. Metal-Insulator Transition in the Dimerized Organic Conductor κ-(BEDT-TTF)$_2$Hg(SCN)$_2$Br. *Phys. Rev. B* **2017**, *96*, 085116. [CrossRef]
59. Pesotskii, S.I.; Lyubovskii, R.B.; Shilov, G.V.; Zverev, V.N.; Torunova, S.A.; Zhilyaeva, E.I.; Canadell, E. Effect of External Pressure on the Metal–Insulator Transition of the Organic Quasi-Two-Dimensional Metal κ-(BEDT-TTF)$_2$Hg(SCN)$_2$Br. *Magnetochemistry* **2022**, *8*, 152. [CrossRef]
60. Hassan, N.; Cunningham, S.; Mourigal, M.; Zhilyaeva, E.I.; Torunova, S.A.; Lyubovskaya, R.N.; Schlueter, J.A.; Drichko, N. Evidence for a Quantum Dipole Liquid State in an Organic Quasi-Two-Dimensional Material. *Science* **2018**, *360*, 1101–1104. [CrossRef]
61. Urai, M.; Miyagawa, K.; Watanabe, Y.; Zhilyaeva, E.I.; Torunova, S.A.; Lyubovskaya, R.N.; Drichko, N.; Kanoda, K. Anomalously Field-Susceptible Spin Clusters Emerging in the Electric-Dipole Liquid Candidate κ-(ET)$_2$Hg(SCN)$_2$Br. *Sci. Adv.* **2022**, *8*, eabn1680. [CrossRef] [PubMed]
62. *CrysAlis PRO Version171.35.19*; Agilent Technologies UK Ltd.: Yarnton, Oxfordshire, UK, 2011.
63. Sheldrick, G.M. IUCr SHELXT—Integrated Space-Group and Crystal-Structure Determination. *Acta Cryst.* **2015**, *A71*, 3–8. [CrossRef]
64. Sheldrick, G.M.; Schneider, T.R. [16] SHELXL: High-Resolution Refinement. *Methods Enzymol.* **1997**, *277*, 319–343. [CrossRef]
65. Hübschle, C.B.; Sheldrick, G.M.; Dittrich, B. ShelXle: A Qt Graphical User Interface for SHELXL. *J. Appl. Cryst.* **2011**, *44*, 1281–1284. [CrossRef] [PubMed]
66. MacRae, C.F.; Sovago, I.; Cottrell, S.J.; Galek, P.T.A.; McCabe, P.; Pidcock, E.; Platings, M.; Shields, G.P.; Stevens, J.S.; Towler, M.; et al. Mercury 4.0: From Visualization to Analysis, Design and Prediction. *J. Appl. Cryst.* **2020**, *53*, 226–235. [CrossRef] [PubMed]
67. Bruno, I.J.; Cole, J.C.; Edgington, P.R.; Kessler, M.; Macrae, C.F.; McCabe, P.; Pearson, J.; Taylor, R. New Software for Searching the Cambridge Structural Database and Visualizing Crystal Structures. *Acta Cryst.* **2002**, *B58*, 389–397. [CrossRef]
68. Ren, J.; Liang, W.; Whangbo, M.-H. *Crystal and Electronic Structure Analysis Using CAESAR*; PrimeColor Software, Inc.: Raleigh, NC, USA, 1998.
69. Saillant, R.; Barcelo, G.; Kaesz, H.D.; Fontal, B.; Bau, R.; Klrtley, S.W.; Churchill, M.R.; Am, J.; Knox, S.A.R.; Koepke, J.W.; et al. The Band Structure of the Tetracyanoplatinate Chain. *J. Am. Chem. Soc.* **2002**, *100*, 6093–6098. [CrossRef]
70. Bardin, A.A.; Kotov, A.I.; Buravov, L.I.; Khasanov, S.S.; Shibaeva, R.P. Metal–Insulator Interplays Rendered by Lattice Transformations and Structural Disorder in DOEO Salts. *Eur. J. Inorg. Chem.* **2014**, *2014*, 4017–4027. [CrossRef]
71. Martin, L.; Day, P.; Clegg, W.; Harrington, R.W.; Horton, P.N.; Bingham, A.; Hursthouse, M.B.; McMillan, P.; Firth, S. Multi-Layered Molecular Charge-Transfer Salts Containing Alkali Metal Ions. *J. Mater. Chem.* **2007**, *17*, 3324–3329. [CrossRef]
72. Martin, L.; Morritt, A.L.; Lopez, J.R.; Akutsu, H.; Nakazawa, Y.; Imajo, S.; Ihara, Y. Ambient-Pressure Molecular Superconductor with a Superlattice Containing Layers of Tris (Oxalato) Rhodate Enantiomers and 18-Crown-6. *Inorg. Chem.* **2017**, *56*, 717–720. [CrossRef]
73. Martin, L.; Lopez, J.R.; Akutsu, H.; Nakazawa, Y.; Imajo, S. Bulk Kosterlitz–Thouless Type Molecular Superconductor β″-(BEDT-TTF)$_2$[(H$_2$O)(NH$_4$)$_2$Cr(C$_2$O$_4$)$_3$]·18-Crown-6. *Inorg. Chem.* **2017**, *56*, 14045–14052. [CrossRef] [PubMed]
74. Morritt, A.L.; Lopez, J.R.; Blundell, T.J.; Canadell, E.; Akutsu, H.; Nakazawa, Y.; Imajo, S.; Martin, L. 2D Molecular Superconductor to Insulator Transition in the β″-(BEDT-TTF)$_2$[(H$_2$O)(NH$_4$)$_2$M(C$_2$O$_4$)$_3$]·18-Crown-6 Series (M = Rh, Cr, Ru, Ir). *Inorg. Chem.* **2019**, *58*, 10656–10664. [CrossRef] [PubMed]
75. Martin, L.; Day, P.; Nakatsuji, S.; Yamada, J.-I.; Akutsu, H.; Horton, P. A Molecular Charge Transfer Salt of BEDT-TTF Containing a Single Enantiomer of Tris(Oxalato)Chromate(III) Crystallised from a Chiral Solvent. *CrystEngComm* **2010**, *12*, 1369–1372. [CrossRef]
76. Rashid, S.; Turner, S.S.; Day, P.; Light, M.E.; Hursthouse, M.B.; Firth, S.; Clark, R.J.H. The First Molecular Charge Transfer Salt Containing Proton Channels. *Chem. Commun.* **2001**, *2001*, 1462–1463. [CrossRef]
77. Akutsu-Sato, A.; Akutsu, H.; Turner, S.S.; Day, P.; Probert, M.R.; Howard, J.A.K.; Akutagawa, T.; Takeda, S.; Nakamura, T.; Mori, T.; et al. The First Proton-Conducting Metallic Ion-Radical Salts. *Angew. Chem.* **2005**, *117*, 296–299. [CrossRef]
78. Coronado, E.; Galán-Mascarós, J.R.; Giménez-Saiz, C.; Gómez-García, C.J.; Triki, S. Hybrid Molecular Materials Based upon Magnetic Polyoxometalates and Organic π-Electron Donors: Syntheses, Structures, and Properties of Bis(Ethylenedithio)Tetrathiafulvalene Radical Salts with Monosubstituted Keggin Polyoxoanions. *J. Am. Chem. Soc.* **1998**, *120*, 4671–4681. [CrossRef]
79. Pénicaud, A.; Boubekeur, K.; Batail, P.; Auban-Senzier, P.; Jérome, D.; Canadell, E. Hydrogen-Bond Tuning of Macroscopic Transport Properties from the Neutral Molecular Component Site along the Series of Metallic Organic-Inorganic Solvates (BEDT-TTF)$_4$Re$_6$Se$_5$Cl$_9$·[Guest], [Guest = DMF, THF, Dioxane]. *J. Am. Chem. Soc.* **1993**, *115*, 4101–4112. [CrossRef]

80. Yoshida, Y.; Ito, H.; Maesato, M.; Shimizu, Y.; Hayama, H.; Hiramatsu, T.; Nakamura, Y.; Kishida, H.; Koretsune, T.; Hotta, C.; et al. Spin-Disordered Quantum Phases in a Quasi-One-Dimensional Triangular Lattice. *Nat. Phys.* **2015**, *11*, 679–683. [CrossRef]
81. Simonov, S.V.; Shevyakova, I.Y.; Zorina, L.V.; Khasanov, S.S.; Buravov, L.I.; Emel'yanov, V.A.; Canadell, E.; Shibaeva, R.P.; Yagubskii, E.B. Variety of Molecular Conducting Layers in the Family of Radical Cation Salts Based on BEDT-TTF with the Metal Mononitrosyl Complex $[OsNOCl_5]^{2-}$. *J. Mater. Chem.* **2005**, *15*, 2476–2488. [CrossRef]
82. Kawamoto, T.; Kurata, K.; Mori, T. A New Dimer Mott Insulator: κ-(BEDT-TTF)$_2$TaF$_6$. *J. Phys. Soc. Jpn.* **2018**, *87*, 083703. [CrossRef]
83. Ginzburg, V.L. Superconductivity and Superfluidity (What Was Done and What Was Not). *Physics-Uspekhi* **1997**, *40*, 407–432. [CrossRef]
84. Matsumiya, S.; Izuoka, A.; Sugawara, T.; Taruishi, T.; Kawada, Y. Effect of Methyl Substitution on Conformation and Molecular Arrangement of BEDT-TTF Derivatives in the Crystalline Environment. *Bull. Chem. Soc. Jpn.* **1993**, *66*, 513–522. [CrossRef]
85. Guionneau, P.; Kepert, C.J.; Bravic, G.; Chasseau, D.; Truter, M.R.; Kurmoo, M.; Day, P. Determining the Charge Distribution in BEDT-TTF Salts. *Synth. Met.* **1997**, *86*, 1973–1974. [CrossRef]
86. Bardin, A.A.; Kotov, A.I. Crystal Structure of Radical-Cation Salt β-(DOET)$_4$CuBr$_4$·PhCl. *Russ. J. Inorg. Chem.* **2006**, *51*, 1886–1891. [CrossRef]
87. Hassan, N.M.; Thirunavukkuarasu, K.; Lu, Z.; Smirnov, D.; Zhilyaeva, E.I.; Torunova, S.; Lyubovskaya, R.N.; Drichko, N. Melting of Charge Order in the Low-Temperature State of an Electronic Ferroelectric-like System. *NPJ Quantum Mater.* **2020**, *5*, 15. [CrossRef]
88. Kushch, N.D.; Bardin, A.A.; Buravov, L.I.; Glushakova, N.M.; Shilov, G.V.; Dmitriev, A.I.; Morgunov, R.B.; Kulikov, A.V. Synthesis Particularities, Structure and Properties of the Radical Cation Salts ω-(BEDT-TTF)$_5$M(SCN)$_6$·C$_2$H$_5$OH, M = Mn, Ni. *Synth. Met.* **2014**, *195*, 75–82. [CrossRef]
89. Clay, R.T.; Mazumdar, S. From Charge- and Spin-Ordering to Superconductivity in the Organic Charge-Transfer Solids. *Phys. Rep.* **2019**, *788*, 1–89. [CrossRef]
90. Allain, M.; Mézière, C.; Auban-Senzier, P.S.; Avarvari, N. Donors for New Molecular Conductors: Combining TMTSF and BEDT-TTF with Anionic $(TaF_6)_{1-x}/(PF_6)_x$ Alloys. *Crystals* **2021**, *11*, 386. [CrossRef]
91. Madalan, A.M.; Canadell, E.; Auban-Senzier, P.; Brânzea, D.; Avarvari, N.; Andruh, M. Conducting Mixed-Valence Salt of Bis(Ethylenedithio)Tetrathiafulvalene (BEDT-TTF) with the Paramagnetic Heteroleptic Anion $[Cr^{III}(Oxalate)_2(2,2'\text{-Bipyridine})]^-$. *New J. Chem.* **2008**, *32*, 333–339. [CrossRef]
92. Kawamoto, T.; Kurata, K.; Mori, T.; Kumai, R. A New Genuine Mott Insulator: β-(BEDT-TTF)TaF$_6$. *J. Phys. Soc. Jpn.* **2021**, *90*, 103703. [CrossRef]
93. Yoshida, Y.; Ito, H.; Maesato, M.; Shimizu, Y.; Hayama, H.; Hiramatsu, T.; Nakamura, Y.; Kishida, H.; Koretsune, T.; Hotta, C.; et al. CCDC 964552 (QUJSAR). Experimental Crystal Structure Determination 2015. Available online: https://doi.org/10.5517/cc11cplp (accessed on 1 October 2023).
94. Simonov, S.V.; Shevyakova, I.Y.; Zorina, L.V.; Khasanov, S.S.; Buravov, L.I.; Emel'yanov, V.A.; Canadell, E.; Shibaeva, R.P.; Yagubskii, E.B. CCDC 258887 (XASCEA). Experimental Crystal Structure Determination 2005. Available online: https://doi.org/10.5517/cc8pd6j (accessed on 1 October 2023).
95. Kawamoto, T.; Kurata, K.; Mori, T. CCDC 1848447 (PIHBIU). Experimental Crystal Structure Determination 2018. Available online: https://doi.org/10.5517/ccdc.csd.cc201gbw (accessed on 1 October 2023).